REVISTA MATÉRIA V.30
ISSN 1517-7076 articles e20250264, 2025

Properties of MWCNTs reinforced activated powder concrete for bridges

Qingping Wang[1], Zhen Wu[1], Xiuxiu Chen[2], Xinchun He[1]

[1]Chengdu Industry & Trade College. Chengdu, Sichuan, China.

[2]Sichuan Central Inspection Technology Inc. Zigong, Sichuan, China.

e-mail: wangqingping@citc-edu.cn, wuzhen@citc-edu.cn, chenxiuxiu@sciti.com.cn, hexinchun@citc-edu.cn

ABSTRACT

The demand for durable concrete in bridge engineering has driven interest in reactive powder concrete (RPC). However, its long-term resistance to sulfate attack remains a concern. This study innovatively enhances RPC's mechanical and corrosion resistance by optimizing the incorporation of 0.12 wt% multi-walled carbon nanotubes (MWCNTs) through a physico-chemical dispersion method (polyvinylpyrrolidone (PVP)-assisted ultrasonication), confirmed to be highly effective. The optimized dispersion achieved a stable Zeta potential of −38.7 ± 1.4 mV after 168 hours. Dry-wet cycling in 12% Na_2SO_4 and $MgSO_4$ simulated sulfate exposure. Key findings show that MWCNT-modified RPC exhibited a 32.98% increase in compressive strength (125.03 MPa) and a 28.19% increase in flexural strength. X-ray computed tomography (X-ray CT) and scanning electron microscopy/energy-dispersive X-ray spectroscopy (SEM-EDS) analyses quantitatively confirm MWCNT-induced pore refinement (51.9% reduction in pore number, 13.55% decrease in porosity) and micro-crack bridging. After 150 Na_2SO_4 cycles, the dynamic elastic modulus loss was 2.13%, while 120 $MgSO_4$ cycles resulted in a 3.25% loss, with mass loss rates below 1%. These findings demonstrate that 0.12 wt% MWCNTs, via the optimized dispersion method, significantly enhance RPC's compactness, crack resistance, and sulfate durability, providing critical technical support for extending the service life of bridge infrastructure in aggressive sulfate environments.

Keywords: MWCNTs; Mechanical properties; Wet-dry cycling; Reactive powder concrete; Sulfate attack; Dispersion.

1. INTRODUCTION

The escalating demand for durable concrete in infrastructure, particularly in bridge construction, necessitates materials that can withstand aggressive environments and prolonged service life [1]. Reactive powder concrete (RPC), distinguished by its remarkable strength and outstanding durability compared to conventional concrete, has emerged as a promising solution. However, even RPC faces challenges in harsh environments, such as those involving high-concentration sulfate exposure and wet-dry cycling, which can lead to microstructural damage and performance degradation [2].

To resolve these issues and further elevate RPC's capabilities, researchers are exploring the incorporation of nanomaterials, including multi-walled carbon nanotubes (MWCNTs). MWCNTs, with their exceptional mechanical properties (high tensile strength and Young's modulus), high aspect ratio, and large surface area, offer the potential to significantly improve concrete's microstructure and resistance to degradation [3]. However, the effective utilization of MWCNTs in cement-based composites faces two major hurdles: (1) the inherent tendency of MWCNTs to agglomerate due to strong van der Waals forces, reducing their reinforcing efficiency, and (2) the limited understanding of their long-term performance under combined mechanical loading and aggressive chemical attack, such as sulfate exposure, conditions frequently encountered in bridge structures [4].

While numerous research efforts have looked into the role of MWCNTs in altering the mechanical properties of cement-based materials [5], many have focused on normal-strength concrete or mortar and have not fully addressed the challenges of achieving stable MWCNT dispersion. For instance, GAO *et al*. [6] demonstrated that MWCNTs could mitigate spalling in concrete at high temperatures, but the study did not delve into the long-term durability under chemical attack. YAMIN *et al*. [7] revealed that incorporating MWCNTs

Corresponding Author: Qingping Wang Received on 23/03/2025 Accepted on 08/09/2025

DOI: https://doi.org/10.1590/1517-7076-RMAT-2025-0264

enhanced the mechanical properties of fly ash concrete, but their work lacked a detailed investigation of dispersion stability and performance in aggressive sulfate environments. RAO *et al*. [8] In order to improve the microstructure, mechanics and durability of recycled concrete aggregates (RCA) in concrete mixed with waste ceramic powder (WCP), 50% attached mortar RCA was preferentially steam-treated with 3% nano-silica (3 hours) Develop a ternary binder mixture of cement, fly ash and WCP and test its performance. The results show that the concrete treated with 30% WCP ternary mixture, 50% attached mortar RCA and 3% nano-silica performs the best, can 100% replace RCA, and the treatment technology is easy to be applied in practice. CHATURVEDY *et al*. [9] aimed to enhance the mechanical properties and high-temperature resistance of rubber concrete by using MWCNTs in combination with rubber aggregates (5%–15%). They optimized the performance through different dosages (0–0.3%) and high-temperature treatment (200–600 °C). The results showed that when 0.2% MWCNTs was added, the compressive strength, flexural strength, and flexural toughness at 28 days increased by 21.91%,10.19%, and 15% respectively compared to the control group. The residual strength at 200°C was significantly improved, but high temperatures (400–600 °C) led to a decrease in strength.

In the study on sulfate-eroded reactive powder concrete, WU *et al*. [10] aimed to enhance the long-term durability of concrete in ammonium sulfate corrosion environments by using recycled plastic to prepare the concrete and analyzing its performance evolution through long-term immersion tests. The results showed that the formation of calcium sulfoaluminate and gypsum during immersion led to continuous expansion and damage of the concrete. Recycled plastic did not improve corrosion resistance but instead exacerbated the long-term erosion damage caused by AS. WU *et al*. [11] investigated the long-term crack evolution of cementitious matrices under sulfate attack by using X-ray dynamic monitoring of ordinary Portland cement (OPC) and resistant to sulfate attack cement (SRPC). The results showed that the volume and depth of cracks in OPC increased significantly over time, indicating severe damage; SRPC suffered less damage. Long-term performance analysis revealed a quadratic relationship between the volume fraction of cracks and the depth of attack. Furthermore, studies specifically addressing sulfate attack resistance of MWCNT-modified RPC are scarce [12, 13]. Existing research often lacks a systematic optimization of the MWCNT dispersion process, a quantitative analysis of the resulting pore structure modifications, and a detailed mechanistic understanding of the MWCNT's role in mitigating sulfate-induced damage [14–18].

This study bridges these gaps by systematically optimizing MWCNT dispersion utilizing polyvinylpyrrolidone (PVP) and ultrasonication, quantitatively analyzing pore structure via X-ray computed tomography (X-ray CT) and scanning electron microscopy and energy-dispersive x-ray spectroscopy (SEM-EDS), and evaluating sulfate resistance under accelerated attack. The findings provide a mechanistic understanding of MWCNTs' role in enhancing both mechanical properties and long-term durability in aggressive environments.

2. MATERIALS AND METHODS

2.1. Materials

This study utilized cementitious materials such as Portland cement (minimum compressive strength of 42.5 MPa), fly ash, ground granulated blast furnace slag (GGBFS), limestone powder, and silica fume. Table 1 provides the chemical composition of each material, as identified through X-ray fluorescence (XRF) analysis.

Table 1: Chemical composition of each cementitious material (mass fraction, %).

CHEMICAL COMPOSITION	FLY ASH	GGBFS	LIMESTONE POWDER	SILICA FUME	PORTLAND CEMENT
SO_3	3.78	1.83	0.52	/	3.81
K_2O	0.82	0.43	0.23	0.65	0.83
Fe_2O_3	3.04	0.64	0.12	0.16	3.05
MgO	4.23	9.25	2.47	0.19	4.15
Na_2O	0.27	0.37	0.13	0.17	0.27
TiO_2	0.37	0.78	0.03	0.02	0.38
Al_2O_3	6.11	15.20	1.47	0.31	5.94
CaO	59.21	36.89	55.00	1.53	59.61
MnO	0.15	0.58	0.11	0.04	0.14
SiO_2	21.92	34.03	40.92	97.93	21.72

Natural river sand (fineness modulus = 2.58) served as the primary aggregate. The MWCNTs (Amresco 308068-56-6) were supplied by Shanghai Yaji Biotechnology Co., Ltd. The as-received MWCNTs had the following properties (as per the manufacturer's specifications): ash content <3%, specific surface area 160–210 g/cm^3, diameter 15–25 nm, length 10–55 μm, purity >90%, and bulk density 0.05–0.1 g/cm^3. Deionized water was implemented for concrete mixing. A melamine-based high-range water reducer (HRWR, water reduction rate = 25%) was implemented to enhance functionality and reduce the water-to-cement ratio [19]. The concrete erosion solution consisted of 12% magnesium sulfate and 12% anhydrous sodium sulfate (both 99% purity).

2.2. MWCNT dispersion procedure

Effective dispersion of MWCNTs is crucial to realize their reinforcing potential in cement-based composites. Due to their elevated aspect ratio and powerful van der Waals interactions, MWCNTs tend to form agglomerates, which act as stress concentrators and hinder the development of a strong interfacial bond with the cement matrix. To overcome this, a combined physico-chemical dispersion method was employed, as illustrated in Figure 1.

This method leverages both mechanical forces (to break down soft agglomerates) and chemical modification (to prevent re-agglomeration). PVP was chosen as the dispersant due to its amphiphilic nature and its ability to interact with MWCNTs through π-π stacking interactions between the pyrrolidone ring of PVP and the MWCNTs. PVP offers advantages over other dispersants due to its non-ionic nature, which minimizes interference with the cement hydration process.

The detailed procedure was as follows:

1) Pre-mixing: MWCNT powder was blended with PVP at a 1: 3 mass ratio in a glass beaker. Deionized water was added to form a slurry.
2) Mechanical stirring: the mixture underwent mechanical stirring via a magnetic stirrer at 1000 rpm for 20 minutes. This step helps to break down large, soft agglomerates.
3) Ultrasonication: the pre-stirred suspension was transferred to a probe sonicator (Hielscher UP400St, 400 W, 24 kHz) and sonicated for 60 minutes at a power density of 300 W/cm^2. The sonication probe was immersed directly into the suspension. The temperature of the dispersion was monitored and maintained below 40 °C utilizing an ice bath to prevent excessive heating, which can degrade the PVP. The high-frequency ultrasonic waves generate cavitation, creating micro-jets that effectively break down hard agglomerates and disperse the MWCNTs individually.

2.3. Preparation of MWCNT-containing concrete

RPC cubes (100 mm × 100 mm × 100 mm) were arranged for compressive strength evaluation, and prisms (300 mm × 100 mm × 100 mm) were arranged for the assessment of dynamic elastic modulus.

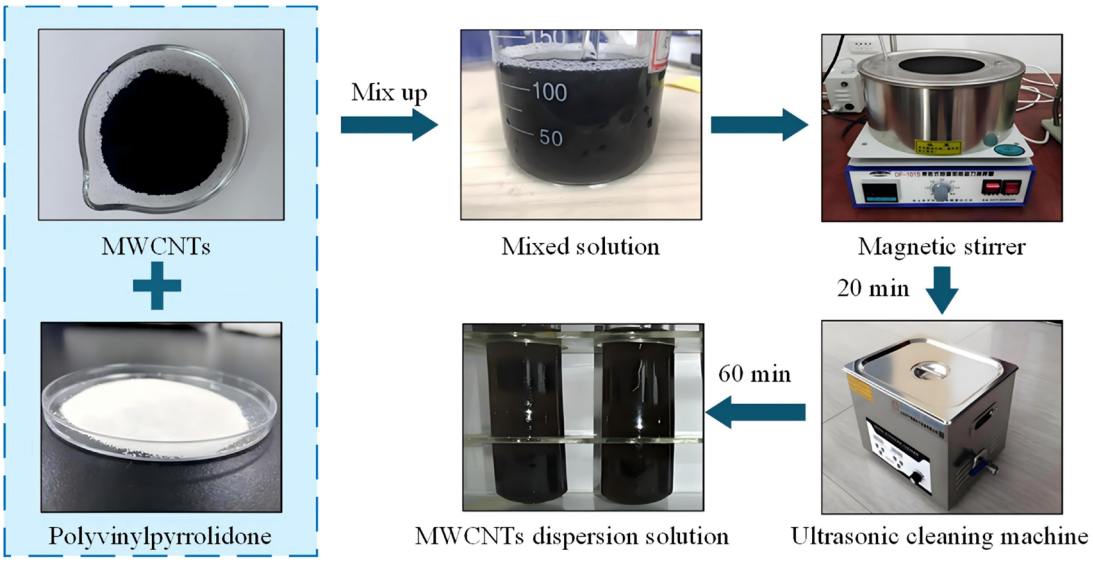

Figure 1: MWCNT dispersion procedure.

Mechanical property testing requires a systematic evaluation of the impact of MWCNTs gradation on strength, hence the use of a benchmark mix (cement 560 kg/m^3, fly ash 160 kg/m^3). The erosion resistance test focuses on the durability of concrete under harsh sulfate environments at the optimal dosage of 0.12%, thus optimizing the mix (increasing cement to 620 kg/m^3, fly ash to 180 kg/m^3). This enhances density and erosion resistance by increasing the amount of binding materials, making the test results more representative of high-durability requirements in actual engineering. Mechanical property testing uses the benchmark mix (superplasticizer 3.0 wt%) to uniformly control the water-to-binder ratio. For the erosion resistance test, which targets the optimal dosage of 0.12 wt%, the total amount of binding materials is increased to enhance density, requiring a simultaneous adjustment of the superplasticizer dosage to 30 kg/m^3 (approximately 4.8 wt%) to maintain flowability and uniformity at a low water-to-binder ratio. The mix proportions are displayed in Table 2.

For the mechanical property tests, MWCNT contents of 0%, 0.04%, 0.08%, 0.12%, 0.16%, 0.20%, and 0.24% (by weight of cementitious materials) were used. For the sulfate attack tests, a 0.12 wt% MWCNT content was selected based on the results of the mechanical property tests.

The mixing procedure was as follows:

1) Dry mixing: cementitious materials (fly ash, GGBFS, limestone powder, silica fume, and Portland cement) and sieved sand (fineness modulus controlled to 2.58) were dry-mixed in a planetary mixer at a speed of 62 rpm for 3 minutes. The target dosage of MWCNT suspension was then added, and dry mixing continued for another 3 minutes at the same speed. This allows the MWCNTs to initially adhere to the surface of the cementitious particles.
2) Wet mixing: the HRWR (pre-mixed with a portion of the deionized water) was incorporated into the dry blend, followed by the remaining deionized water. The mixture was then wet-mixed at a speed of 125 rpm for 5 minutes. The water-to-cementitious materials ratio was maintained at 0.18.
3) Molding and curing: the fresh concrete was cast into molds and vibrated on a vibrating table (frequency = 50 Hz) for 2 minutes to remove entrapped air. The specimens were then covered with plastic sheets and maintained at ambient temperature (23 ± 2 °C) for 24 hours. After being taken out of the molds, the specimens underwent curing in a room maintained at 20 ± 2 °C and a relative humidity of no less than 95% for 28 days. Specimens for sulfate attack testing were cured for an additional 2 days (30 days total).

2.4. Characterization methods

2.4.1. X-ray CT

X-ray CT was implemented to obtain three-dimensional images of the concrete microstructure. A Nikon VOXLS 30 C 225 CT scanner was implemented with the following parameters: voxel resolution = 10 μm^3, X-ray voltage = 120 kV, current = 150 μA, exposure time = 500 ms/frame, angular interval = 0.18°. The Avizo software (version 9.0) was implemented for image processing and analysis.

Table 2: Mix proportions of raw materials for various test specimens (kg/m^3).

COMPOSITION OF COMPONENTS	MECHANICAL PROPERTIES TEST SAMPLE	SULFATE ATTACK TEST SAMPLE
Fly ash	160	180
GGBFS	120	120
Limestone powder	80	80
Silica fume	100	100
Portland cement	560	620
Sand	1100	1200
Water reducing agent (wt.%)	3.0	30
Water-cement ratio	0.18	0.18
Mwcnts (wt.% of cementitious materials)	0/0.04/0.08/0.12/0.16/0.20/0.24	0.12
Water (kg/m^3)	155	160

The image processing involved the following procedures:

Region of interest (ROI) selection: a cubic region (80 mm × 80 mm × 80 mm) was cropped from the center of each scanned specimen to eliminate edge artifacts.

Noise reduction: a median filter (3 × 3 × 3 kernel) was applied to reduce noise while preserving edge sharpness.

Segmentation: interactive thresholding was implemented to segment the pores from the solid matrix. The threshold value was determined based on the histogram of grayscale values and visual inspection of the resulting binary images. The same thresholding criteria were applied to all specimens to ensure consistency.

Pore analysis: Avizo's "Label Analysis" module was implemented to quantify the number, volume, and spatial distribution of pores.

2.4.2. SEM-EDS

SEM was implemented to examine the microstructure of the concrete and the MWCNT-cement matrix interface. Small samples (approximately 10 mm × 10 mm × 5 mm) were extracted from the fractured surfaces of the specimens after mechanical testing. To stop hydration, the samples were immersed in anhydrous ethanol for 24 hours. The samples were then dried in a vacuum oven at 40 °C until constant weight. Prior to SEM imaging, the samples were coated with a thin layer of gold (approximately 10 nm thick) utilizing a sputter coater (Quorum Q150R ES) to enhance conductivity [20].

A Hitachi S-4800 field emission scanning electron microscope (FE-SEM) was implemented for imaging. EDS analysis utilized an Oxford Instruments X-Max detector attached to the SEM to confirm the presence and distribution of MWCNTs within the cement matrix. High-magnification images (up to 50,000×) were acquired to visualize the MWCNT-cement matrix interface and the crack-bridging effect. Image J software was implemented to measure crack widths from the SEM images.

2.5. Performance testing methods

2.5.1. Mechanical property testing

Compressive and flexural strength tests were conducted in accordance with the Chinese standard GB/T 50081-2019 utilizing an HY-1080 electronic universal material testing apparatus. The loading rates were 0.5 MPa/s for compressive strength and 0.06 MPa/s for flexural strength. For each examination, at least three specimens were tested, and the average value and standard deviation were reported [21].

The relative dynamic elastic modulus E_r was calculated utilizing Equation 1.

$$E_r = \frac{E_b}{E_a} \times 100\% \tag{1}$$

where E_b denotes the dynamic elastic modulus after n wet-dry cycles, and E_a denotes the initial dynamic elastic modulus.

The dynamic elastic modulus ($E_{dynamic}$) was evaluated utilizing the resonance frequency method, as per Equation 2.

$$E_{dynamic} = k \cdot \frac{\rho L^4 f^2}{I} \tag{2}$$

where k denotes a correction factor (dependent on specimen shape), ρ denotes the material density, L denotes the specimen length, f denotes the resonance frequency, and I denotes the cross-section's moment of inertia.

2.5.2. Sulfate attack resistance testing

The sulfate attack resistance was evaluated utilizing a wet-dry cycling procedure. The cured concrete specimens (30 days old) were subjected to cycles of immersion in a sulfate solution (12% Na_2SO_4 + 12% $MgSO_4$) for 12 hours, followed by drying in an oven at 60 ± 2 °C for 12 hours, and then cooling in air at ambient temperature (23 ± 2 °C) for 1 hour. This cycle was repeated up to 150 times. The 60 ± 2 °C drying temperature was chosen based on previous research [22] to accelerate the sulfate attack process while avoiding the decomposition of ettringite, which typically occurs above 70 °C. This temperature allows for the formation of expansive products

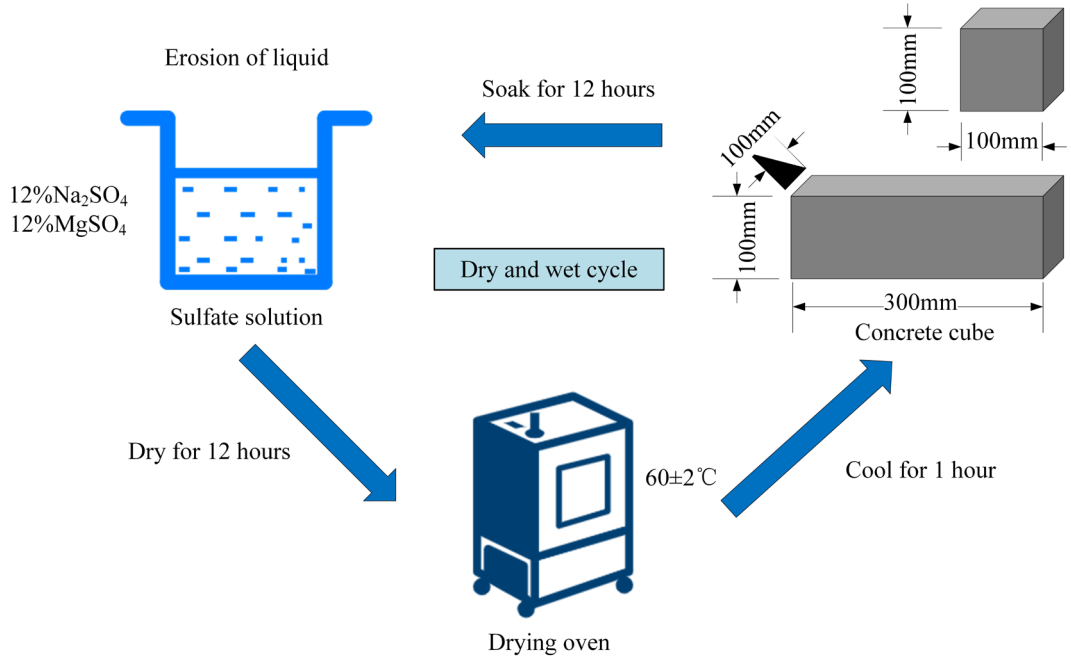

Figure 2: Wet-dry cycle erosion process of RPC cubes.

(ettringite and gypsum) without causing significant thermal damage to the C-S-H gel. The 12-hour immersion and drying durations were selected to allow sufficient time for both sulfate ion penetration and the formation of expansive products, based on preliminary tests and literature recommendations. The specific wet-dry process is detailed in Figure 2.

After specific numbers of cycles, the specimens underwent testing for compressive strength, dynamic elastic modulus, and mass loss. Compressive strength was evaluated at intervals of 0, 20, 40, 60, 80, 100, 120, and 150 cycles. To provide a more detailed analysis of damage evolution, the relative dynamic elastic modulus and mass loss were measured more frequently, specifically at every 10 cycles up to 120 cycles, with a final measurement at 150 cycles for the Na_2SO_4 test.

3. RESULTS

3.1. MWCNT dispersion quality

The effectiveness of the combined physico-chemical dispersion method was evaluated utilizing Zeta potential measurements. Zeta potential quantifies the electrostatic potential at the slipping plane in a colloidal dispersion, and its magnitude indicates the degree of electrostatic repulsion between particles. A higher absolute value of Zeta potential (typically above |30| mV) indicates a more stable dispersion, as the repulsive forces prevent particle agglomeration.

As illustrated in Table 3, the synergistically dispersed group (PVP + ultrasonication) exhibited a significantly higher initial Zeta potential (–41.3 ± 1.5 mV) compared to the untreated group (–12.5 ± 1.2 mV) and the physically dispersed group (–19.8 ± 0.8 mV). This indicates a much stronger electrostatic repulsion between the MWCNTs in the synergistically dispersed group. After 168 hours, the Zeta potential of the synergistically dispersed group remained high (–38.7 ± 1.4 mV), well above the stability threshold of |30| mV, with minimal sedimentation (<5%). In contrast, the physically dispersed group showed a rapid decrease in Zeta potential and significant agglomeration, while the untreated group exhibited complete stratification. These outcomes clearly illustrate the success of the combined physico-chemical approach in achieving a stable and well-dispersed MWCNT suspension. While the Zeta potential confirms the stability of the initial suspension, its primary role in this study is as a quality control parameter to ensure the nanotubes are introduced into the cement matrix in a well-dispersed state. The final, effective dispersion and its positive impact on the microstructure within the hardened concrete are subsequently verified by the SEM-EDS and X-ray CT analyses.

3.2. Effect of MWCNTs on mechanical properties

Figure 3 illustrates the impact of MWCNT content on the compressive and flexural strength of RPC. Error bars represent the standard deviation from the mean of three specimens. As illustrated in Figure 3a, the compressive

Table 3: Zeta potential test results.

GROUP	T0 H POTENTIAL (MV)	T24 H POTENTIAL (MV)	T72 H POTENTIAL (MV)	T168 H POTENTIAL (MV)	STABILITY AFTER STANDING (168 H)
Untreated group	−12.5 ± 1.2	−10.1 ± 1.5	−8.3 ± 2.1	−5.6 ± 1.8	Complete stratification (settlement >95%)
Physical dispersion group	−19.8 ± 0.8	−17.2 ± 1.1	−15.1 ± 0.9	−12.7 ± 1.3	Significant agglomeration (turbidity↑↑, ~40% sedimentation)
Synergistic dispersion group	−41.3 ± 1.5	−40.5 ± 1.2	−40.0 ± 0.9	−38.7 ± 1.4	Slight turbidity change (<5% sedimentation)

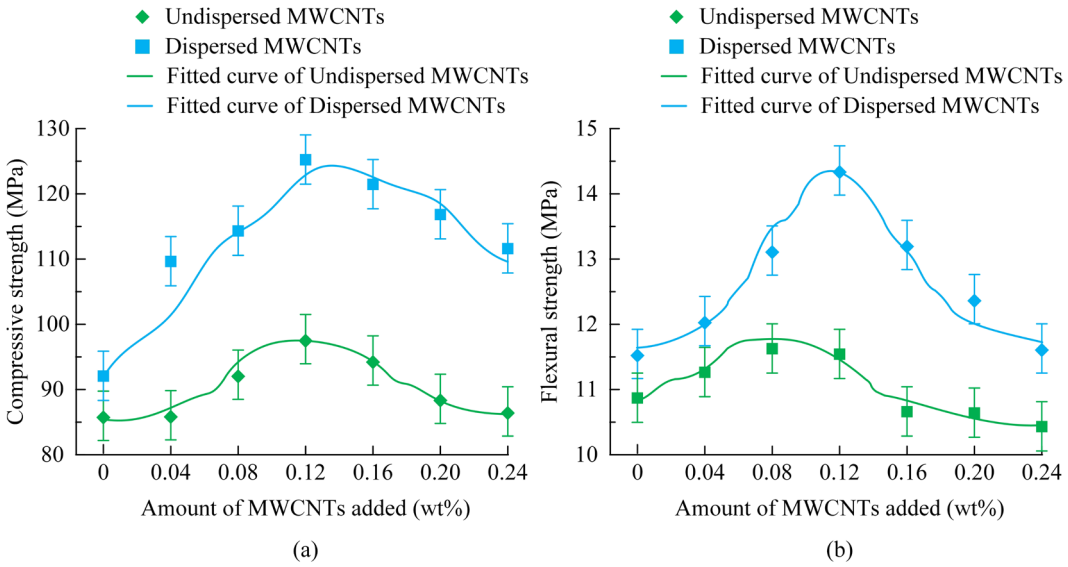

Figure 3: Effect of MWCNT content on (a) compressive strength and (b) flexural strength mechanical properties of RPC.

strength of the RPC initially increased with increasing MWCNT content, reaching a maximum value of 125.03 MPa at 0.12 wt% dispersed MWCNTs. This represents a 32.98% increase compared to the control group (94.02 MPa) and a 28.18% increase compared to the group with undispersed MWCNTs (97.54 MPa). Beyond 0.12 wt%, the compressive strength decreased, likely due to the increased probability of MWCNT agglomeration at higher concentrations, creating weak zones within the matrix. The compressive strength of concrete with undispersed MWCNTs was consistently lower than that of concrete with dispersed MWCNTs at all addition amounts, highlighting the importance of proper dispersion. Gaussian single-peak function fitting showed a strong correlation between compressive strength and dispersed MWCNT content ($R^2 = 0.9956$).

Figure 3b demonstrates a similar trend for flexural strength. The maximum flexural strength (14.37 MPa) was also achieved at 0.12 wt% dispersed MWCNTs, representing a 31.54% increase compared to the control group (10.92 MPa) and a 28.19% increase compared with the maximum flexural strength of concrete with undispersed MWCNT (11.21 MPa).

The enhancement in mechanical properties can be attributed to several mechanisms: 1) Crack bridging: MWCNTs, with their high tensile strength and aspect ratio, can bridge micro-cracks, hindering their propagation and increasing the energy required for fracture; 2) Pore refinement: MWCNTs can fill nano-scale pores within the cement matrix, reducing the overall porosity and increasing the density of the material; 3) Improved interfacial bonding: the well-dispersed MWCNTs create a larger interfacial area with the cement hydration products, leading to a stronger bond and improved load transfer. These mechanisms are further supported by the SEM and X-ray CT results presented below.

To verify the mechanical performance enhancement effect of 0.12 wt% MWCNTs (ultrasonically dispersed with PVP) on RPC, this study selected four typical MWCNTs/CNTs reinforcement systems from existing

Table 4: Comparison of mechanical properties of composites under different MWCNTs reinforcement systems.

STUDY TYPE	MWCNTS TYPE AND DOSAGE	COMPRESSIVE STRENGTH (MPa)	FLEXURAL STRENGTH (MPa)
This Study	0.12 wt% MWCNTs (PVP + ultrasonic dispersion)	125.03	14.37
Reference [23]	0.5 wt% Nickel-coated MWCNTs	167.7	14.3
Reference [24]	0.075 vol% Ni-CNTs (aspect ratio 1000)	108.8	8.2
Reference [25]	0.075 vol% Ni-CNTs (aspect ratio 125)	89.5	7.7
Reference [26]	0.1 wt% CNTs + 0.3% PPF	124.3	13.9

literature for comparison, focusing on the absolute differences in compressive strength and flexural strength. The mechanical property comparisons of composites under different MWCNTs reinforcement systems are shown in Table 4.

As shown in Table 4, the RPC prepared by 0.12 wt% MWCNTs (treated with PVP+ ultrasonic dispersion) in the study demonstrated certain advantages in compressive strength (125.03 MPa) and flexural strength (14.37 MPa) under low dosage conditions. Compared with the 0.5 wt% nickel-coated MWCNTs (compressive strength 167.7 MPa, flexural strength 14.3 MPa) in Literature 1, although the compressive strength of the studied material is slightly lower, the amount of MWCNTs is only 24% of it, and the flexural strength is basically the same, demonstrating high reinforcement efficiency. The reinforcing effects of the two length-to-diameter ratios of Ni-CNTs (0.075 vol%) in Reference [2] were both weak (compressive strength ≤108.8 MPa, flexural strength ≤8.2 MPa). Compared with the composite system (0.1 wt% CNTs+0.3% PPF) in reference [4], the research shows that a single doping of MWCNTs can achieve similar compressive strength (125.03 MPa vs 124.3 MPa) and higher flexural strength (14.37 MPa vs 13.9 MPa), verifying that a single nanomaterial can replace the multi-component reinforcement scheme under specific dispersion conditions. Overall, the research has achieved an efficient improvement in the mechanical properties of RPC by optimizing the dispersion method while reducing the amount of nanomaterials used, providing an economically feasible technical path for the application of high-performance composite materials in bridge engineering.

3.3. Microstructural analysis

The distribution of the main elements and SEM images of MWCNTs in the RPC with dispersed MWCNTs are displayed in Figure 4. Figure 4a demonstrates the distribution of carbon, calcium, silicon, and oxygen elements in the concrete, and Figure 4b demonstrates the effect of 0.12 wt% MWCNTs in the concrete. As illustrated in Figure 4a, the main elements in the concrete are uniformly distributed, indicating that the MWCNTs, after the combined physico-chemical treatment, are relatively uniformly dispersed in the concrete. As illustrated in Figure 4b, MWCNTs can densify the porous parts of the concrete through filling and bridge the cracks in the concrete, thereby improving the mechanical properties of the concrete. During the mixing process, MWCNTs migrate to the surface of the aggregate along with water, forming an interfacial transition zone (ITZ) enriched with nanonucles, and creating a low-density C-S-H phase induced by nanonucles. This phase has higher hardness and modulus, bridging the mechanical gap between the aggregate and the cement paste. The crack bridging observed in Figure 4b directly results from the densification caused by this ITZ.

After X-ray CT processing of the concrete samples, Avizo was implemented to obtain the pore structure of the samples, As illustrated in Figure 5. Figure 5a demonstrates the pore structure of concrete without MWCNTs, and Figure 5b demonstrates the pore structure of concrete with 0.12 wt% dispersed MWCNTs. Figure 5 visually demonstrates that there are more pores in the concrete without MWCNTs, while the number and size of pores in the concrete with 0.12 wt% dispersed MWCNTs are significantly reduced. Calculations utilizing Avizo showed that the number of pores in the concrete without MWCNTs was 12623, with a porosity of 2.73%, while the number of pores in the concrete with 0.12 wt% dispersed MWCNTs was 6072, with a porosity of 2.36%. Compared to the concrete without MWCNTs, the number of pores decreased by 51.90%, and the porosity decreased by 13.55%.

The cumulative pore size distribution and pore volume fraction of the concrete are displayed in Figure 6. Figure 6a demonstrates the cumulative pore size distribution, and Figure 6b demonstrates the pore volume fraction. As illustrated in Figure 6a, the number of pores with a volume of 1 mm^3 or less in the concrete without MWCNTs is significantly greater than that in the concrete with 0.12 wt% dispersed MWCNTs, and there are only a few pores with a volume greater than 1 mm^3. This indicates that the bridging and filling effects of

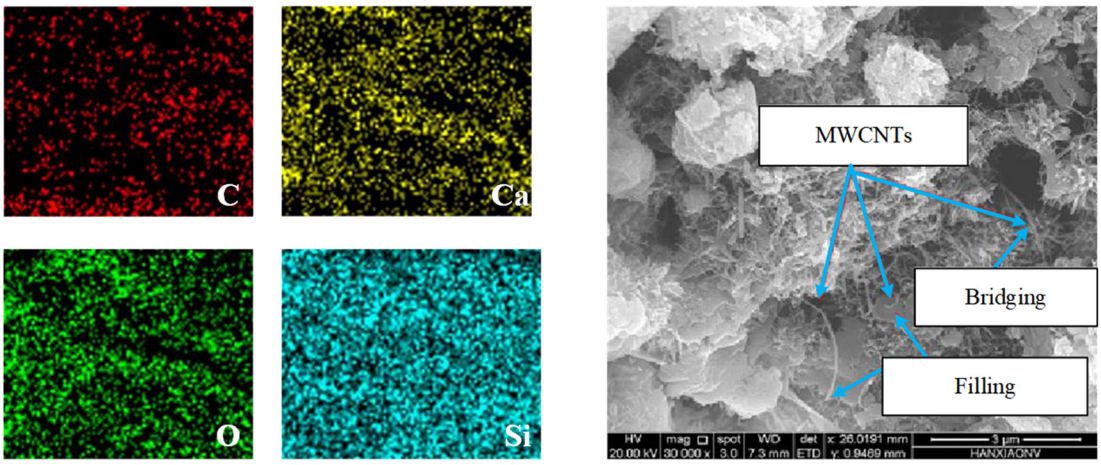

Figure 4: (a) Distribution of main elements (C, Ca, Si, O) in RPC and (b) SEM images of MWCNTs bridging and filling effect.

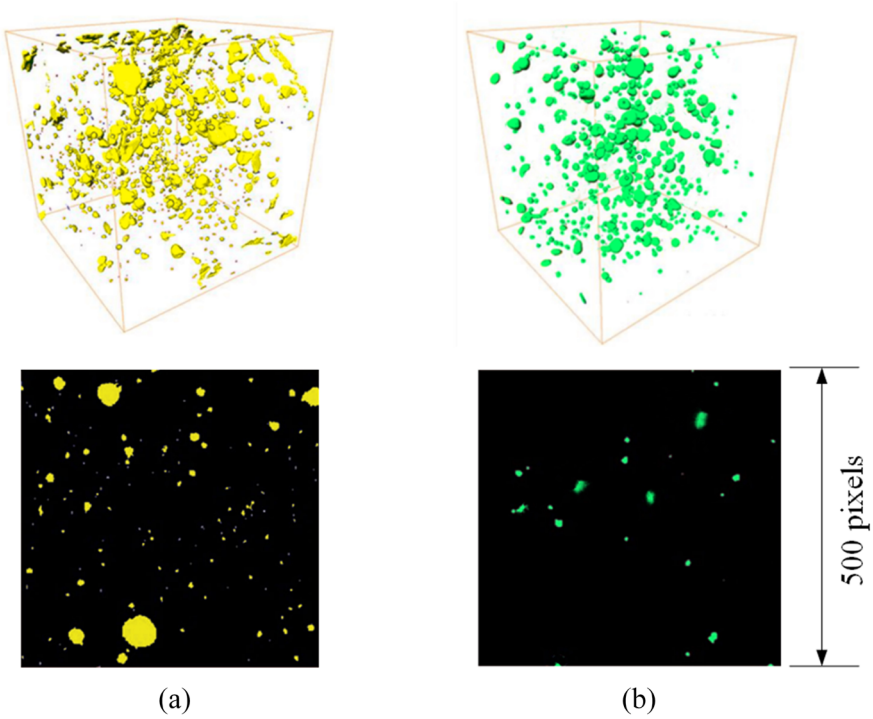

Figure 5: Pore structure of concrete with (a) 0% MWCNTs and (b) 0.12 wt% dispersed MWCNTs.

MWCNTs can effectively fill the pores in the concrete. As illustrated in Figure 6b, the fluctuation amplitude of the pore volume fraction in each X-Y plane of the concrete with MWCNTs is significantly lower than that of the concrete without MWCNTs. This indicates that MWCNTs, while filling the pores in the concrete, also make the distribution of pore volume more uniform within the concrete. This is mainly because MWCNTs, as nucleation sites for the formation of C-S-H gels, accelerate early hydration, promote the generation of high-density C-S-H phases, and simultaneously reduce the content of low-density C-S-H, thereby leading to a decrease in porosity and pore refinement. Quantitative analysis of SEM images through Avizo software showed that the proportion of spherical/nearly spherical pores (aspect ratio ≤1.5) in 0.12 wt.% MWCNTs modified RPC increased from 42% in the control group to 68%, while the proportion of irregular fissure pores decreased from 35% to 12%. According to the theory of mechanics of materials, the stress concentration coefficient of spherical pores ($K_t \approx 2$) is significantly lower than that of irregular pores ($K_t > 3$), which can effectively reduce the stress concentration effect under load and thereby decrease the probability of microcrack initiation.

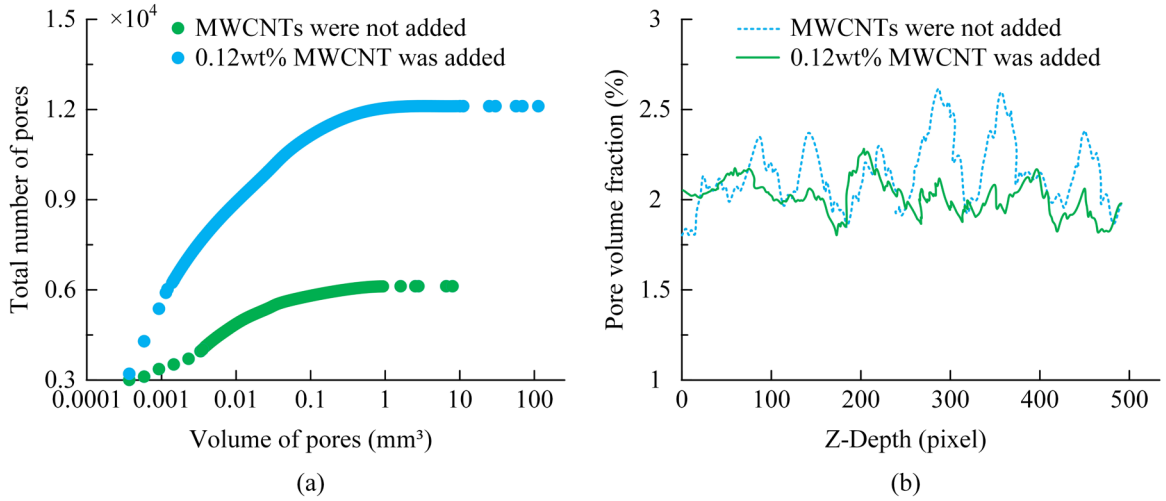

Figure 6: Pore structure analysis of (a) cumulative pore size distribution and (b) pore volume fraction.

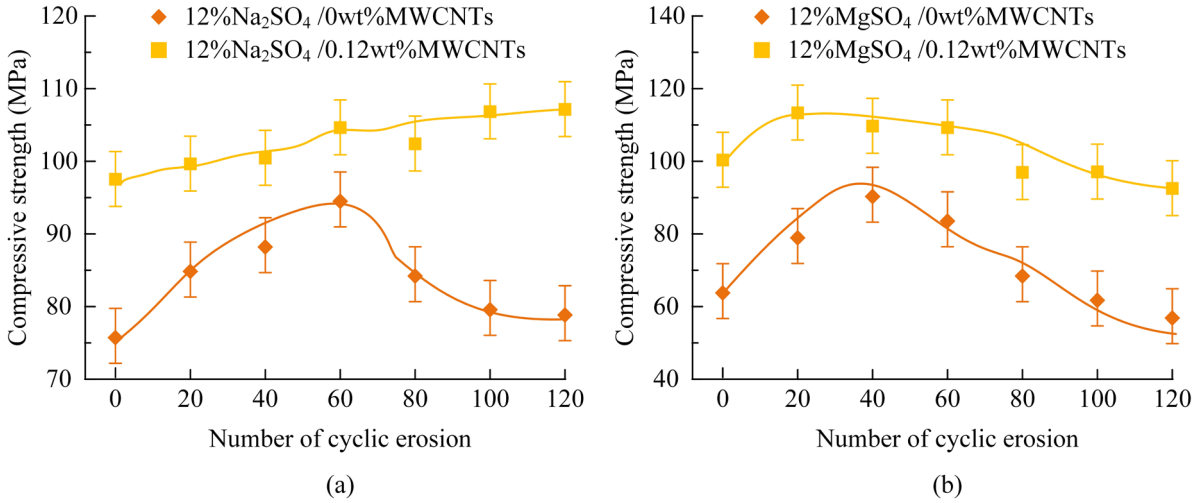

Figure 7: Compressive strength changes with (a) 12% Na_2SO_4 solution and (b) 12% $MgSO_4$ solution erosion cycles.

3.4. Effect of MWCNTs on the sulfate attack resistance of RPC

To analyze the sulfate attack resistance of concrete with MWCNTs, the prepared concrete samples were cured for 30 days and then subjected to erosion tests utilizing high-concentration sulfate solutions according to the wet-dry cycle method described above. The changes in compressive strength of the concrete under different test conditions with the number of erosion cycles are displayed in Figure 7. Figure 7a demonstrates the changes in compressive strength of concrete samples with and without MWCNTs when eroded in a 12% Na_2SO_4 solution, and Figure 7b demonstrates the changes in compressive strength when eroded in a 12% $MgSO_4$ solution.

As illustrated in Figure 7a, in the 12% Na_2SO_4 solution, the compressive strength of the specimens without MWCNTs gradually increased during the first 60 erosion cycles, while the compressive strength of the specimens with MWCNTs also increased, but the increase was lower than that of the former. This is because, during hydration, the formation and growth of ettringite crystals fill the pore network inside the specimens, thereby enhancing the compactness and mechanical properties of the specimens. Moreover, the sulfate ion reacts with calcium hydroxide in concrete to produce expansive calcium aluminite, which can fill the pores in the interior of concrete and improve the density, thus enhancing the compressive strength. As the number of erosion cycles increased, the compressive strength of the specimens without MWCNTs gradually decreased but remained higher than the compressive strength before erosion. This is due to the excessive expansion of calcium aluminate, which leads to internal stress concentration and triggers microcrack propagation. In addition, magnesium ions in magnesium

sulfate undergo ion exchange reactions with C-S-H gel, causing its decomposition and structural damage. This decomposition weakens the internal structure of concrete, leading to a decrease in compressive strength. The compressive strength of the specimens with MWCNTs gradually increased with the increasing number of erosion cycles. This is because the addition of MWCNTs concrete significantly reduces the number and porosity of pores through pore filling and crack bridging, limits the infiltration path of erosion fluid, and delays the decomposition of hydration products and the expansion of microcracks, thus showing higher strength stability in the later stage of erosion. As illustrated in Figure 7b, in the 12% $MgSO_4$ solution, the compressive strength of the specimens with and without MWCNTs gradually increased before the 20th and 40th erosion cycles, respectively. As the number of erosion cycles increased, the compressive strength of both decreased, and the decrease in the specimens with MWCNTs was smaller. This indicates that the $MgSO_4$ solution has a greater impact on the compressive strength of concrete, while the addition of MWCNTs makes the compressive strength of the specimens more stable.

The effect of MWCNTs on the concrete surface is displayed in Figure 8. As illustrated in Figures 8a, 8b, and 8c, when eroded in the 12% Na_2SO_4 solution, the surface of the concrete specimens with 0.12 wt% MWCNTs did not show significant damage compared to the specimens without MWCNTs, indicating a lower number of formed pores. As illustrated in Figures 8d, 8e, and 8f, when eroded in the 12% $MgSO_4$ solution, the number and depth of pores on the surface of the specimens without MWCNTs increased significantly, while the specimens with MWCNTs still maintained a relatively smooth surface.

The variation of the relative dynamic elastic modulus of the MWCNTs test block with the number of erosions (0-120 times, a total of 13 data points, spaced 10 cycles) is shown in Figure 9. Figures 9a and 9b depict the changes in relative dynamic elastic modulus of the specimens in 12% Na_2SO_4 and 12% $MgSO_4$ solutions, respectively.

As illustrated in Figure 9, in the 12% Na_2SO_4 solution, the relative dynamic elastic modulus of the concrete, regardless of whether MWCNTs were added, showed a trend of first increasing and then decreasing. In the initial increasing stage, the SO_4^{2-} in the erosion medium reacted with $Ca(OH)_2$ in the concrete to form expansive ettringite, filling pores and increasing compactness, leading to an increase in dynamic elastic modulus. This process was accompanied by an increase in pore connectivity. As the number of erosion cycles increased, the concrete without MWCNTs experienced stress concentration and microcrack propagation due to excessive ettringite expansion and the ion exchange reaction of C-S-H gel, leading to a significant decrease in dynamic elastic modulus. The concrete with MWCNTs, through the pore-filling effect, reduced the diameter of the concrete pores, reducing the penetration channels for the erosion solution. Furthermore, the high strength of the

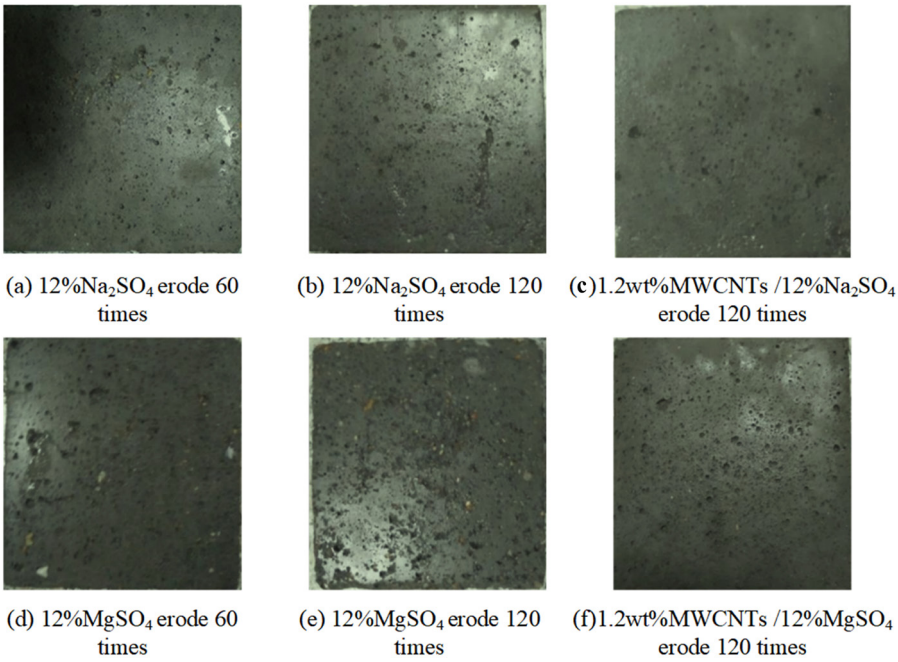

Figure 8: Effects of concrete surfaces after sulfate attack with (a) 12% Na_2SO_4 erode 60 times, (b) 12% Na_2SO_4 erode 120 times, (c) 1.2 wt% MWCNTs/12% Na_2SO_4 erode 120 times, (d) 12% $MgSO_4$ erode 60 times, (e) 12% $MgSO_4$ erode 120 times and (f) 1.2 wt% MWCNTs/12% $MgSO_4$ erode 120 times.

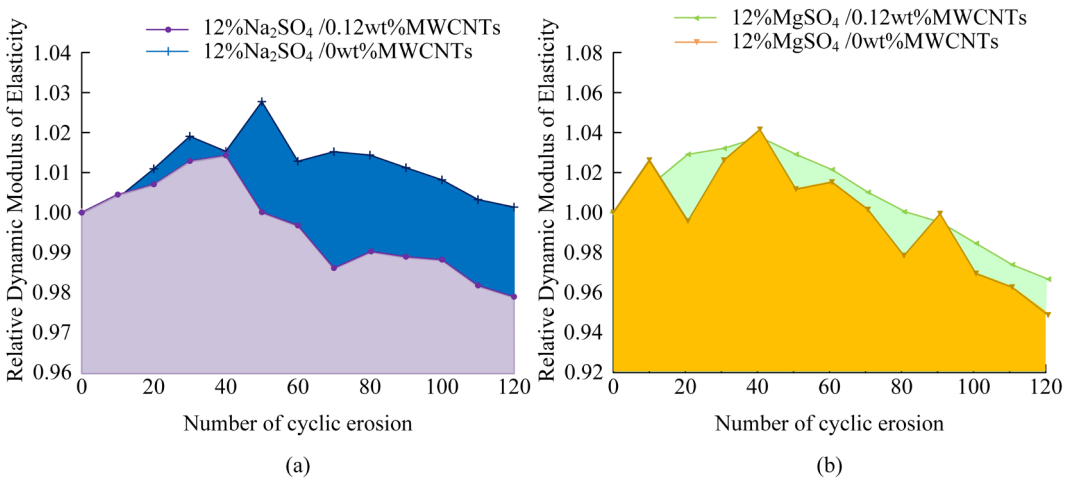

Figure 9: Effect of MWCNTs on the relative dynamic elastic modulus of concrete with (a) 12% Na_2SO_4 solution and (b) 12% $MgSO_4$ solution erosion cycles.

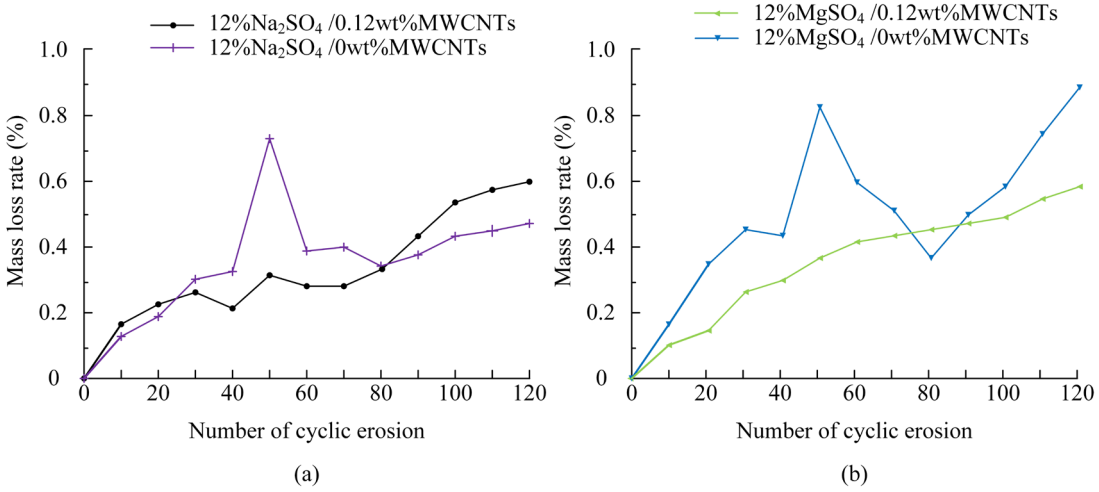

Figure 10: Concrete mass loss curves with (a) 12% Na_2SO_4 solution and (b) 12% $MgSO_4$ solution erosion cycles.

MWCNTs restricted crack propagation through a bridging effect. The relative dynamic elastic modulus of the specimens with MWCNTs decreased by 2.13% after 150 erosion cycles compared to the initial value.

In the 12% $MgSO_4$ solution, the relative dynamic elastic modulus of the specimens with MWCNTs began to decrease after the 40th erosion cycle, and after 120 erosion cycles, it ultimately decreased by 3.25%.

The changes in mass loss of concrete with and without MWCNTs with the number of erosion cycles are displayed in Figure 10. Figures 10a and 10b depict the mass loss curves of concrete in 12% Na_2SO_4 and 12% $MgSO_4$ solutions, respectively. As illustrated in Figure 10, the mass loss rate of all specimens was less than 1% after 120 erosion cycles. The growth rate of the mass loss rate of the concrete with MWCNTs was relatively slow. After 120 erosion cycles, the 12% $MgSO_4$ solution caused more mass loss to the specimens than the 12% Na_2SO_4 solution. MWCNTs are uniformly dispersed on the concrete surface, forming a dense network layer that reduces the direct contact between the sulfate solution and the matrix, thereby reducing the mass loss of the concrete. Simultaneously, MWCNTs adsorb the PVP dispersant through π-π conjugation, increasing the surface charge density and inhibiting the adsorption and reaction of SO_4^{2-} and Mg^{2+}, delaying the formation of erosion products. Overall, the addition of MWCNTs to the specimens significantly reduced the impact of sulfate attack.

4. DISCUSSION

This study systematically investigated the influence of well-dispersed MWCNTs on the mechanical properties and sulfate attack resistance of RPC. The combined physico-chemical dispersion method utilizing PVP and

ultrasonication ensured stable dispersion, as confirmed by Zeta potential measurements. An optimal MWCNT dosage of 0.12 wt% significantly enhanced compressive and flexural strength, attributed to crack bridging, pore refinement, and improved interfacial bonding, as evidenced by SEM, EDS, and X-ray CT analyses.

The MWCNT-modified RPC exhibited superior sulfate resistance, demonstrating lower strength loss, reduced porosity, and mitigated micro-crack formation under Na_2SO_4 and $MgSO_4$ wet-dry cycling. The improvement in durability is largely due to the reduced permeability and refined microstructure, preventing expansive sulfate-induced damage. These findings align with MOGHADAM *et al*. [27], who reported an optimal MWCNT dosage range of 0.10–0.15 wt% for enhanced durability. However, unlike previous studies, our research emphasizes a rigorous dispersion optimization process and provides quantitative microstructural evidence. While KAN *et al*. [28] focused primarily on mechanical properties, our study expands the scope by addressing sulfate attack resistance. Similarly, KUMAR *et al*. [29] explored self-sensing properties rather than durability, further distinguishing this research.

Despite these promising results, further investigations are necessary to explore the long-term durability of MWCNT-modified RPC under realistic environmental conditions, particularly in the presence of chloride ingress and freeze-thaw cycles. The effects of different MWCNT functionalization strategies, such as acid treatment or silane coupling, should be examined to optimize dispersion stability and interfacial bonding. Additionally, integrating MWCNTs with other nanomaterials, such as graphene oxide or nanosilica, may yield synergistic enhancements in mechanical properties and durability. To facilitate practical implementation, multi-scale modeling approaches should be developed to predict RPC performance, optimize mix designs, and assess service life. Moreover, conducting a life cycle assessment would provide insights into the environmental impact and economic feasibility of incorporating MWCNTs in RPC for infrastructure applications. Finally, understanding the rheological behavior of fresh RPC is essential to ensure workability and ease of placement in large-scale construction projects. These future directions will contribute to a deeper understanding of MWCNT-modified RPC and its potential for durable and sustainable infrastructure development.

5. CONCLUSION

This study demonstrated that the incorporation of well-dispersed MWCNTs significantly enhances both the mechanical properties and sulfate attack resistance of RPC. A combined physico-chemical dispersion method, employing PVP and ultrasonication, was crucial for achieving a stable MWCNT dispersion. The optimal MWCNT dosage was found to be 0.12 wt% (by weight of cementitious materials), resulting in substantial improvements in compressive strength (32.98% increase) and flexural strength (28.19% increase) compared to the control RPC.

The enhancement mechanisms were attributed to crack bridging, pore refinement, and improved interfacial bonding between the MWCNTs and the cement matrix, as confirmed by X-ray CT and SEM with EDS. The MWCNT-modified RPC exhibited superior resistance to both Na_2SO_4 and $MgSO_4$ attack, with significantly lower reductions in compressive strength and dynamic elastic modulus, and reduced mass loss during accelerated wet-dry cycling tests. Specifically, after 150 cycles in 12% Na_2SO_4, the MWCNT-modified concrete showed a dynamic elastic modulus loss of only 2.13%, and after 120 cycles in 12% $MgSO_4$, the loss was 3.25%; both exhibited mass loss rates below 1%. These improvements are attributed to the reduced permeability, enhanced crack resistance, and improved microstructure provided by the well-dispersed MWCNTs.

This research provides valuable insights into the design and development of high-performance, durable concrete for bridge applications. The findings demonstrate the significant potential of MWCNTs to mitigate sulfate-induced degradation and extend the service life of concrete structures in aggressive environments. The optimized dispersion method and the quantitative microstructural analysis presented in this study provide a foundation for further research and the practical implementation of nanotechnology in concrete construction.

6. BIBLIOGRAPHY

[1] ELMOGHAZY, Y., ABUELGASIM, E.M.O., OSMAN, S.A., *et al*., "Effective mechanical properties evaluation of unidirectional and bidirectional composites using virtual domain approach at microscale", *Archives of Advanced Engineering Science*, v. 1, n. 1, pp. 27–37, Oct. 2023. doi: http://doi.org/10.47852/bonviewAAES32021723.

[2] BIRADAR, A., KANDASAMY, J., "Influence of varied MWCNTs dispersion on EMI shielding, UV absorption, and surface properties of electroless NiP/MWCNT-coated UHMWPE fabric", *Fibers and Polymers*, v. 25, n. 4, pp. 1367–1389, Apr. 2024. doi: http://doi.org/10.1007/s12221-024-00502-x.

[3] LIU, Y., ZHANG, C., CAI, K., *et al*., "Application of carbon nanotubes in ultra-fine cement grouts", *Bulletin of the Chinese Ceramic Society*, v. 42, n. 07, pp. 2309–2316, 2023.

[4] DAI, J., WEI, D., WANG, Z., *et al*., "Comparative research on atomic diffusion of diamond/Ni and MWCNTs/Ni interfaces with molecular dynamics and experimental methods", *Ceramics International*, v. 51, n. 4, pp. 5434–5450, Feb. 2025. doi: http://doi.org/10.1016/j.ceramint.2024.12.191.

[5] ANH, T.N., NGOC, T.N., "Soft ground improvement below bridge approach foundation using cement deep mixing columns combined with geotextile", *Journal of Applied Engineering Science*, v. 21, n. 2, pp. 491–500, Apr. 2023. doi: http://doi.org/10.5937/jaes0-40629.

[6] GAO, F., TIAN, W., CHENG, X., "Study on spalling and cracking behavior of MWCNTs concrete exposed to high temperatures", *Structural Concrete*, v. 24, n. 3, pp. 3220–3235, Jun. 2023. doi: http://doi.org/10.1002/suco.202200716.

[7] YAMIN, W., JUNFENG, D., LI, Z., *et al.* "Effect of multi-walled carbon nanotubes on mechanical and durability of fly ash concrete", *Journal of Functional Materials/Gongneng Cailiao*, v. 55, n. 9, Sep. 2024. http://doi.org/10.3969/j.issn.1001-9731.2024.09.029.

[8] RAO, A.U., SHETTY, P.P., BHANDARY, R.P., *et al*., "Assessment of fly ash and ceramic powder incorporated concrete with steam-treated recycled concrete aggregates prioritising nano-silica", *Emergent Materials*, v. 7, n. 2, pp. 443–472, Apr. 2024. doi: http://doi.org/10.1007/s42247-024-00639-8.

[9] CHATURVEDY, G.K., BASHAR, N., PANDEY, U.K., "Incorporating multi-walled carbon nanotubes in rubberized concrete: impact on physical, mechanical, and fire resistance properties", *Fullerenes, Nanotubes, and Carbon Nanostructures*, v. 32, n. 12, pp. 1121–1134, Dec. 2024. doi: http://doi.org/10.1080/1536383X.2024.2375597.

[10] WU, H., ZHAO, C., ZHANG, Z., *et al*., "Deterioration behavior of recycled plastic concrete corroded by ammonium sulfate solution", *ACI Materials Journal*, v. 120, n. 3, pp. 117–127, May. 2023. doi: http://doi.org/10.14359/51738687.

[11] WU, M., CAO, K., XIAO, W., *et al*., "Experimental observing damage evolution in cement pastes exposed to external sulfate attack by In Situ X-Ray computed tomography", *Journal of Wuhan University of Technology*, v. 40, n. 1, pp. 164–170, Feb. 2025. doi: http://doi.org/10.1007/s11595-025-3050-7.

[12] SONG, S., NIU, Y., KONG, L., "Correlation analysis of pore structure and frost resistance of carbon nanotube concrete based on gray relational theory", *Structural Concrete*, v. 25, n. 4, pp. 2855–2867, Aug. 2024. doi: http://doi.org/10.1002/suco.202300222.

[13] JAYAKUMARI, B.Y., SWAMINATHAN, E.N., PARTHEEBAN, P., "Sustainable construction material using nanosilica and multi-walled carbon nanotubes in cement concrete", *Advances in Nano Research*, v. 16, n. 5, pp. 459–472, May. 2024.

[14] SAKTHIESWARAN, N., MOORTHY, N., RENISHA, M., *et al*., "Optimization of strength properties of reactive powder concrete by response surface methodology", *Journal of Shanghai Jiaotong University (Science)*, v. 29, n. 5, pp. 900–908, Jun. 2024. doi: http://doi.org/10.1007/s12204-023-2612-0.

[15] XIE, Y., WANG, Y., ZHANG, B., *et al*., "Mechanical properties of steel-reinforced reactive powder concrete columns with different geometrical dimensions after high-temperature exposure", *International Journal of Civil Engineering*, v. 22, n. 9, pp. 1623–1641, Sep. 2024. doi: http://doi.org/10.1007/s40999-024-00967-0.

[16] ZHU, P., ZHU, Y., QU, W., *et al*., "Stress-strain relationship for reactive powder concrete with recycled powder under uniaxial compression", *Frontiers of Structural and Civil Engineering*, v. 18, n. 7, pp. 1015–1027, Jul. 2024. doi: http://doi.org/10.1007/s11709-024-1063-5.

[17] HUYNH, T., NGO, S., NGUYEN, V., "A modified reactive powder concrete made with fly ash and river sand: an assessment on engineering properties and microstructure", *Periodica Polytechnica. Civil Engineering*, v. 68, n. 4, pp. 1031–1039, 2024. doi: http://doi.org/10.3311/PPci.23912.

[18] HIREMATH, P., "Performance of reactive powder concrete with different fiber varieties at higher temperatures and retention periods", *Magazine of Concrete Research*, v. 76, n. 14, pp. 805–815, Feb. 2024. doi: http://doi.org/10.1680/jmacr.23.00191.

[19] BHATROLA, K., MAURYA, S.K., KOTHIYAL, N.C., "Research on the influence of dispersed carbon nanomaterials with different water reducing agent in cementitious mortar", *Fullerenes, Nanotubes, and Carbon Nanostructures*, v. 32, n. 6, pp. 561–576, Jun. 2024. doi: http://doi.org/10.1080/1536383X.2024.2306806.

[20] GU, J., LI, J., LI, L., *et al*., "Effect of Sputtering Technology on Microstructure and Mechanical Properties of TiN Coatings", *Surface Technology*, v. 52, n. 09, pp. 160–169, 2023.

[21] NATIONAL STANDARD OF THE PEOPLE'S REPUBLIC OF CHINA. *GB/T 50081-2002 Standard for test method of mechanical properties on ordinary concrete*, Beijing, GB, 2003.

[22] GONG, J., YANG, Q., GUO, L., *et al*., "Performance of alkali-activated slag-glass powder based foamed concrete", *Bull. Chin. Ceram. Soc*, v. 41, pp. 226–234, 2022. doi: http://doi.org/10.16552/j.cnki.issn1001-1625.2022.01.025.

[23] CUI, X., HAN, B., ZHENG, Q., *et al*., "Mechanical properties and reinforcing mechanisms of cementitious composites with different types of multiwalled carbon nanotubes", *Composites. Part A, Applied Science and Manufacturing*, v. 103, n. 12, pp. 131–147, Dec. 2017. doi: http://doi.org/10.1016/j.compositesa.2017.10.001.

[24] DONG, S., WANG, D., ASHOUR, A., *et al*., "Nickel plated carbon nanotubes reinforcing concrete composites: from nano/micro structures to macro mechanical properties", *Composites. Part A, Applied Science and Manufacturing*, v. 141, pp. 106228, Feb. 2021. doi: http://doi.org/10.1016/j.compositesa.2020.106228.

[25] XING, G., XU, Y., HUANG, J., *et al*., "Research on the mechanical properties of steel fibers reinforced carbon nanotubes concrete", *Construction & Building Materials*, v. 392, pp. 131880, Aug. 2023. doi: http://doi.org/10.1016/j.conbuildmat.2023.131880.

[26] ALGAIFI, H.A., MUHAMMAD, E.A., BAHAROM, S., *et al*., "Optimizing polypropylene fiber and carbon nanotubes to reinforce concrete matrix: a response surface methodology", *Construction & Building Materials*, v. 442, pp. 137388, 2024. doi: http://doi.org/10.1016/j.conbuildmat.2024.137388.

[27] MOGHADAM, H.A., NESHAEI, S.A., MIRHOSSEINI, S.M., *et al*., "Durability characteristics and mechanical properties of multi-walled carbon nanotubes reinforced concrete, a case study: Caspian seawater curing condition", *European Journal of Environmental and Civil Engineering*, v. 27, n. 1, pp. 140–158, Jan. 2023. doi: http://doi.org/10.1080/19648189.2022.2031303.

[28] KAN, D., LIU, G., CHEN, Z., *et al*., "Mechanical properties and microcosmic mechanism of multi-walled carbon nanotubes reinforced ultra-high strength concrete", *Fullerenes, Nanotubes, and Carbon Nanostructures*, v. 31, n. 2, pp. 157–167, Feb. 2023. doi: http://doi.org/10.1080/1536383X.2022.2130899.

[29] KUMAR, C.A., REDDY, P.N., AEJAZ, S., *et al*., "Self-sensing concrete with recycled coarse aggregates and multi-walled carbon nanotubes: a sustainable and effective method", *Research on Engineering Structures & Materials*, v. 10, n. 1, pp. 41–56, Jan. 2024. doi: http://doi.org/10.17515/resm2023.773ma0520.